A SLAG TEMPERATURE AND FLOW MONITORING SYSTEM

Jean-Philippe Andreu

Joanneum Research, Institute of Digital Image Processing, Wastiangasse 6, A-8010 Graz, Austria

Abstract: Quality assessment of steel processing essentially relies on the continuous monitoring and control of the steel temperature and the flow patterns of the molten material. Among the various sensors developed to control that process, CCD cameras emerge as a good alternative to more classical measuring devices. Multi-spectral imaging systems based on cameras working in the visible spectrum offer a viable alternative to high cost thermographic infrared cameras. This paper presents a slag monitoring system based on dual wavelength thermographic cameras. The system allows a real-time and contactless monitoring of the slag temperature and a continuous monitoring of the flow patterns of the ingot slag topping in order to assess the quality of the produced steel.

1   INTRODUCTION

Precisely controlling the solidification of liquid steel is one of the cornerstones in quality steel making. By varying the amount of heating, usually by adjusting the current going through an electrode immersed the liquid steel one can precisely control the solidification process. This is why monitoring the temperature of the liquid phase of the steel is of great importance to steel producers.

Given the very high temperatures of liquid steel and the slag on top of it (usually between 1300°C and 1800°C) and the particularly harsh environment at the producing plant, only very few sensors (usually thermocouple probes and pyrometers) are able to accurately measure the temperature of the steel. Conventionally, for measuring the temperature an operator has to immerse a probe with a thermocouple into the liquid steel slag at periodic intervals. Since thermocouple probes cannot work reliably under the influence of the high currents, the heating electrode has to be removed from the mould before a measurement is done. This periodic removal of heating power disturbs the solidification process. An alternative way of measuring the temperature was therefore sought, provided that it can guarantee at least the same accuracy as thermocouple probes: +/- 5 °C.

Due to their high cost thermographic infrared cameras were often discarded as an option. At a fraction of the cost of infrared cameras a dual wavelength camera solution working in the visible spectrum offers a viable alternative (Meriaudeau, 2003). Such a system can deliver images of high spatial resolution while at the same time measuring temperature with an accuracy better than +/- 5 °C. Using thermal cameras is also beneficial to the observation of the flow patterns of the molten material. That important process information was until now only estimated by a trained operator.

Still it is pretty hard to determine the temperature of liquid steel from images. Within an image of the surface one can see regions where the material forms a "crust" (i.e. "cold" regions), while other regions display a laminar flow of hot material from below up to the surface with from time to time spontaneous "bubbles" bringing up hot liquid at a fast rate. One of the difficult tasks for an image processing algorithm is therefore to distinguish those areas and at the same time yield a accurate temperature.

2   TEMPERATURE MEASURE

2.1   Monochromatic Method

Contactless temperature measurement is based on the analysis of the radiations emitted by the object under inspection. Planck's law relates the

electromagnetic energy radiated from a black body to its absolute temperature:

$$L_\lambda^0(T) = \frac{C_1}{\pi\lambda^5} \cdot \frac{1}{\exp\left(\dfrac{C_2}{\lambda T_\lambda^0}\right) - 1} \qquad (1)$$

with T_λ^0 the temperature, λ the wavelength, $\frac{C_1}{\pi\lambda^5}$ the first radiation constant: 1.191062×10^8 Wμm^{4}sr^{-1}, C_2 the second radiation constant: 1.438786×10^4 Wμm and L_λ^0 the spectral radiance. As ideal emitter a black body emits the maximum radiation compared to any other object for a given temperature. The non-ideal behaviour of real objects is generally accounted by the emissivity ε_λ. It corresponds, for the same spectral wavelength λ, to the ratio of the actually emitted total radiation to its theoretical maximum (i.e. black body radiation). Since $\varepsilon_\lambda \leq 1$ the apparent temperature of a real object measured by a radiometer is always lower than its true temperature. A derivation of Eq. (1) is then used to determine the true target temperature T_λ^t from the measured temperature T_λ^m:

$$\frac{1}{T_\lambda^t} = \frac{1}{T_\lambda^m} + \frac{\lambda}{C_2} \ln \varepsilon_\lambda \qquad (2)$$

Due to surface properties and experimental conditions determining a reliable value for ε_λ can prove a difficult and error prone task.

2.2 Dual-wavelength Method

Measuring temperature with a dual wavelength method was first introduced by Campbell et al. (Campbell, 1925). The method consists in measuring the ratio of two spectral radiances. Using spectral filters, two radiances emitted by the object are acquired simultaneously at two different wavelengths λ_1 and λ_2. The temperature $T_{\lambda_1,\lambda_2}^t$ is then inferred from the ratio temperature $T_{\lambda_1,\lambda_2}^R$:

$$\frac{1}{T_{\lambda_1,\lambda_2}^t} = \frac{1}{T_{\lambda_1,\lambda_2}^R} + \frac{\lambda_R}{C_2} \ln \varepsilon_R \qquad (3)$$

λ_R being the ratio wavelength: $\lambda_R = \dfrac{\lambda_1\lambda_2}{\lambda_2 - \lambda_1}$ (4)

ε_R being the ratio emissivity: $\varepsilon_R = \dfrac{\varepsilon_{\lambda_1}}{\varepsilon_{\lambda_2}}$ (5)

And $\dfrac{1}{T_{\lambda_1,\lambda_2}^R} = \lambda_R\left(\dfrac{1}{\lambda_1 T_{\lambda_1}^m - \lambda_2 T_{\lambda_2}^m}\right)$ (6)

According to Eq. (3), the ratio temperature $T_{\lambda_1,\lambda_2}^R$ corresponds to the true target temperature $T_{\lambda_1,\lambda_2}^t$ whenever ε_{λ_1} and ε_{λ_2} are equal (i.e. $\varepsilon_R = 1$) which is the definition of a gray body.

2.3 System Layout

Urban et al. (Urban, 2005), following Meriaudeau et al. (Meriaudeau, 2003), presented a temperature measurement system composed of a beam splitter and two CCD cameras equipped with different interferential filters. That system, based on dual wavelength, estimates the temperature of gray bodies with a maximum error of 0.5% of the experimental temperature range with the assumption that the emissivity does not change too much as a function of the wavelength (i.e. gray body assumption). In other words, ε_{λ_1} and ε_{λ_2} have to be chosen sufficiently close from each other while at the same time distant enough to allow sufficient sensitivity of the instrument.

That system has several advantages. As long as the gray body assumption holds the measured object and the calibration object do not need to be of the same material. This means the measuring instrument can be calibrated with one radiation source (e.g. a tungsten filament inside a lamp bulb) but can then be used to measure the temperature of another object of totally different material (e.g. the molten slag). Another advantage of the dual wavelength approach is its inherent robustness with regard to dust. Dust depositing on the front lens will equally influence intensities measured at both wavelengths and therefore does not deteriorate the measurement accuracy.

2.4 Practical Considerations

Under immediate vicinity to the melting process the system must still reliably perform under environmental challenges such as:

- Extreme heat radiation from the melted steel: The camera system is built into a massive housing, an extra air cooled radiation shield is needed to keep the cameras within their specified operating temperature range (i.e. below 50°C).
- Extremely strong magnetic fields in the vicinity of the melting electrode: Proper choice of location and heavy magnetic shielding of the

camera housing and the cabling have to be taken into account.

- High levels of dust / smoke during the process: All the sensitive optics and electronics have been built into a fully sealed housing while a circular ventilation slit around the first optical element in the system (heat protection filter) avoids deposition of dust.
- Gears occluding the camera field of view: The gear manipulating the heating electrode can temporarily occlude the camera field of view therefore the measurement location has to be chosen with care.

Because calibrated blackbodies were only available up to 1500°C and the temperatures under consideration are above the fusion point for most metals an alternative approach was chosen to calibrate the instrument up to 2000°C. The relationship between the temperature and the current of a 250 W halogen lamp was established using a classic Hartmann und Braun filament pyrometer. The tungsten filament of the halogen bulb was used as a rough calibration. For better accuracy a NIST traceable black body can be used for calibration.

2.5 Temperature Measurement Results

Temperature measurement results are shown in Figure 1. The curves represent about 2.5 hours of the process at a sampling rate of one measurement per second. The deep notches in the temperature curves show the influence of a thermocouple measurement: when the electrode is taken out, the fluid steel circulation stops resulting in a sharp drop in surface temperature. The upper curve represents the measurement of the hottest spot (typically a bubble rising from below the slag surface). The lower curve displays the average temperature over the whole liquid steel surface. That curve correlates quite well with thermocouple measurements. The most precise measurements come from measuring the temperature from areas that are reliably visible at all stages of the process such as large laminar flowing areas that bring up to the surface a continuous stream of hot material.
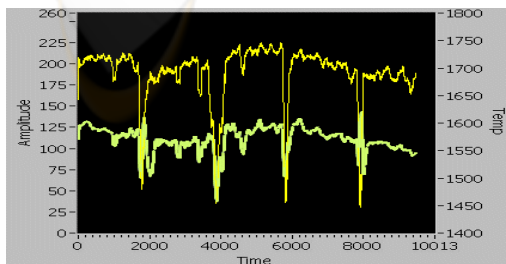

Figure 1: Temperature measurement results.

3 FLOW MONITORING

During the steel producing process the flow pattern of the slag is a visible indicator of the process quality. Currently a worker checks on an irregular basis the slag motion and interprets its motion. In a qualitative manner the motion can be specified as 'good' if the direction of the homogeneous slag is flowing towards the electrode from all directions. On the other hand if the slag flows from the centre of the electrode towards the border of the mould the slag motion is qualified as 'bad'.

3.1 Active Slag Region of Interest

To speed up the qualitative slag motion computation we restrict ourselves to the most active regions where the most active motion will be observed.

Contrary to regions where the slag is solidified (i.e. cold slag), active regions are the hottest and therefore correspond to the regions with the highest intensity in the images of the slag. Segmenting these regions is simply performed by an optimal thresholding method (Otsu, 1979) and by discarding the regions of too small area. Figure 2 shows the segmentation result on a test image.
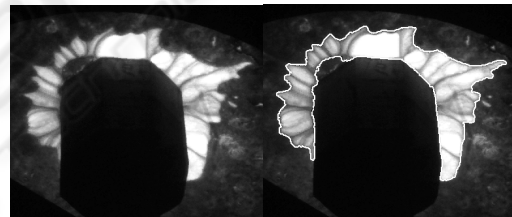

Figure 2: Segmented image region of slag active motion.

3.2 Slag Motion Analysis

In an image sequence the moving patterns of the slag cause temporal variations of the image brightness. If we assume that all temporal intensity changes are due to motion only, analysing the slag motion requires to compute how much each image pixel moves between adjacent images. For determining the motion parameters we use a pyramidal variant (Bouguet, 2000) of the well-known tracking algorithm presented by Lucas and Kanade (Lucas, 1981). This algorithm was chosen because it is general enough, reliable, robust and fast enough to handle the required frame rate of our monitoring system.

504

3.2.1 Motion Tracking

The basis of the Motion Constraint Equation assumes that if $I(x, y)$ is the centre pixel of neighbourhood Ω and moves by a displacement vector $\vec{d} = (\delta x, \delta y)$ within an adjacent image J (with $J = I(\delta t)$), since $I(x, y)$ and $J(x + \delta x, y + \delta y)$ represent the same point one can write:

$$I(x, y, t) = I(x + \delta x, y + \delta y, t + \delta t) \qquad (7)$$

Providing that δx, δy and δt are not too big, one can perform a first order Taylor series expansion about $I(x, y, t)$:

$$(7) = I(x, y, t) + \frac{\partial I}{\partial x}\delta x + \frac{\partial I}{\partial y}\delta y + \frac{\partial I}{\partial t}\delta t + \varepsilon \qquad (8)$$

where ε is assumed to be small and can be neglected. Using Eq. (7) and Eq. (8) we obtain:

$$I_x \upsilon_x + I_y \upsilon_y + I_t = 0 \qquad (9)$$

Where $\upsilon_x = \dfrac{\delta x}{\delta t}$ and $\upsilon_y = \dfrac{\delta y}{\delta t}$ are the components of the image velocity and $I_x = \dfrac{\partial I}{\partial x}$, $I_y = \dfrac{\partial I}{\partial y}$ and $I_t = \dfrac{\partial I}{\partial t}$ are the image intensity derivatives. Eq. (9) can be rewritten more compactly as:

$$\nabla I \cdot \vec{\upsilon}^T = -I_t \qquad (10)$$

where $\nabla I = (I_x, I_y)$ is the spatial intensity gradient and $\vec{\upsilon} = (\upsilon_x, \upsilon_y)$ is the image velocity or optical flow at pixel (x, y) at time t.

A weighted least-squares fit of the local first-order constraints of Eq. (10) to a constant model for $\vec{\upsilon}$ in each small spatial neighbourhood Ω can be implemented by minimizing:

$$\sum_{x, y \in \Omega} W^2(x, y)\left[\nabla I(x, y, t) \cdot \vec{\upsilon}^T + I_t(x, y, t)\right]^2 \qquad (11)$$

where $W(x, y)$ denotes a window function that gives more influence to constraints at the centre of the neighbourhood than those at the periphery. $W(x, y)$ are typically 2D Gaussian coefficients but can be set to 1.0 with little effect on the accuracy. The solution to Eq. (11) is given by:

$$\vec{\upsilon} = \left[A^T A\right]^{-1} A^T \vec{b} \qquad (12)$$

where for N pixels in Ω at a single time t:

$$A = \left[\nabla I(x_1, y_1), ..., \nabla I(x_N, y_N)\right] \qquad (13)$$

$$\vec{b} = -\left(I_t(x_1, y_1), ..., I_t(x_N, y_N)\right) \qquad (14)$$

The solution to Eq. (12) can be solved in closed form when $A^T A$ is a non-singular matrix:

$$A^T A = \begin{bmatrix} \sum\limits_{x, y \in \Omega} I_x^2(x, y) & \sum\limits_{x, y \in \Omega} I_x(x, y)I_y(x, y) \\ \sum\limits_{x, y \in \Omega} I_y(x, y)I_x(x, y) & \sum\limits_{x, y \in \Omega} I_y^2(x, y) \end{bmatrix} \quad (15)$$

3.2.2 Accuracy and Robustness

The two key components for determining the optical flow are accuracy and robustness. The accuracy component relates to the ability of taking into account the details contained in the images. Intuitively, a small neighbourhood Ω would be preferable in order not to "smooth out" image details. The robustness component relates to the sensitivity to changes of lighting, size of image motion, etc... In particular, in order to handle large motions, it is intuitively preferable to pick a large neighbourhood Ω. Therefore there is a natural trade-off between local accuracy and robustness when choosing the neighbourhood size.

In order to provide a solution to that problem, we use a pyramidal implementation of the classical Lucas-Kanade algorithm (Bouguet, 2000). In that variant implementation an image pyramid is first built by recursively sub-sampling (by a factor of 2) the highest resolution image up to a user defined pyramid height/level L_m. The optical flow is computed at the deepest pyramid level L_m and propagated to the upper levels up to level 0 (the original image). The final solution $\vec{d}$ is the sum of the residual pixel displacement vectors available after the finest optical flow computation: $\vec{d} = \sum\limits_{L=0}^{L_m} 2^L \vec{d}^L$. The clear advantage of a pyramidal implementation is that it allows large pixel displacements, while keeping the size of the neighbourhood relatively small.

3.2.3 Differentiation

Image intensity derivatives are required for computing the optical flow. Differentiation is done using matched balanced filters (Simoncelli, 1994) of

size 5 for low pass filtering (e.g. blurring) and high pass filtering (e.g. differentiation). Matched filters allow comparisons between the signal and its derivatives as the high pass filter is simply the derivative of the low pass filter and, from experimental observations, yields more accurate derivative values.

For instance for computing I_x, we first convolve with the low pass filter in the t dimension to reduce 5 images to one, then convolve that image with the same filter in the y dimension and finally convolve with the differentiation filter in the x dimension to obtain I_x.

3.2.4 Tracking Points

Instead of tracking all the points within areas where the slag is active, we limit ourselves to tracking featured points. Following Shi and Tomasi (Shi, 1994) the selection of featured points is more than a traditional measure of "interest": it is determining the right features that make the tracker work best.

A measure of "textureness" is derived over non-overlapping square windows of size 15 in the areas of interest. That measure is based on the assumption that if the inter-frame displacement is sufficiently small with respect to the texture fluctuations within the window, the displacement vector can be found minimizing the error residue:

$$\varepsilon = \int_\Omega \left[I\left(x - \vec{d}\right) - J(x) \right]^2 w\, dx \qquad (16)$$

In this expression, w is a weighting function and could be set to 1 or alternatively, could be a Gaussian-like function that emphasizes the central area of the window. Solving that linear system requires the coefficients to be both above the image noise level and well conditioned. Using Singular Value Decomposition (SVD) for solving the system and one can decide by examining the resulting eigen values (e.g. the smallest of the eigen values should be superior to a user specified threshold) if the system well conditioned and if the window is a valid one for that measure.

In order to avoid tracking too many feature points we restrict their number to a user defined value (e.g. from 600 to 1000). To prevent the feature points to be crowded in some few spots, which results in a poor distribution of trackable points (see Figure 3), we use a parameter to specify the desired minimum distance (in pixels) between the candidate points. Experience showed that using a minimum distance of 4 pixels delivers good results in well distributing the points. Increasing this factor too

much results in poor tracking resolution because the points get spread too far apart.
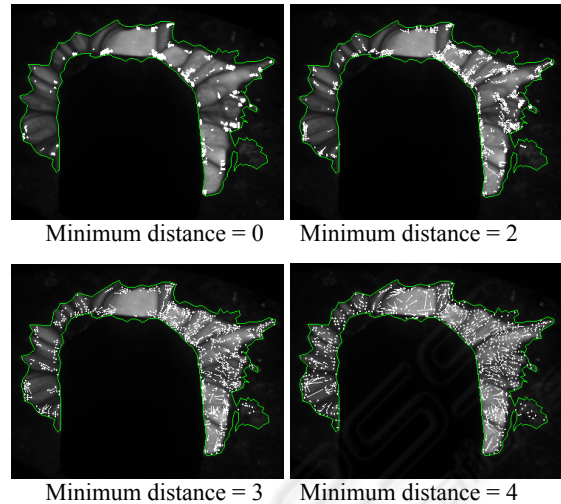

Minimum distance = 0   Minimum distance = 2

Minimum distance = 3   Minimum distance = 4

Figure 3: Effect of different minimum distance values on tracking point distribution.

3.2.5 Re-initialisation of Tracking Points

During the tracking process the algorithm tries to track every feature point found at the initialization step over the next frames. If the point is lost for instance by moving out of the active slag area or by not being identified again in the new frame, the algorithm initializes (using the procedure described in the previous section) a new point for the one lost to keep the total number of tracking points constant.

3.3 Finding the Electrode Centre

Before analyzing the overall slag motion we first have to define a reference point, which the motion of the slag can be related to. We use the approximate centre of the electrode as reference point.

Starting from the resulting image mask by segmenting the region of active slag motion (Figure 4 left), this mask contour is first converted into a polygon. From this polygonal representation the convex hull is computed.

The convex hull of a set of points is the intersection of all convex sets containing that set. For N points $P_1, ..., P_N$ the convex hull is then given by the expression:

$$C \equiv \left\{ \sum_{j=1}^N \lambda_i p_j : \lambda_i \geq 0, \forall j \text{ and } \sum_{j=1}^N \lambda_i = 1 \right\} \qquad (17)$$

From the convex hull the centre of mass (Figure 4 right) is computed and taken as an approximation for the centre of the electrode which is used to relate

the direction of the tracking vectors for analysing the slag motion.

Figure 4: The electrode centre as the convex hull centroid.

3.4 Direction of the Slag Flow

To determine the overall slag motion, the region of active slag motion is divided into sectors of a circle centred at the approximated electrode centre (Figure 5). The number of sectors and the distance between them is user dependant. Experiments showed that in combination with 600 to 1000 tracking points, 12 sectors delivered good results.

Within each sector the tracking vectors are accumulated into a histogram of directions. To improve robustness in detecting the main direction in each sector we do not take into account vectors whose length do not exceed 3 pixels. Finding the maximum in the directional histogram provides the preferred direction of the slag motion of the considered sector. Figure 5 displays the main directions found for each sector.
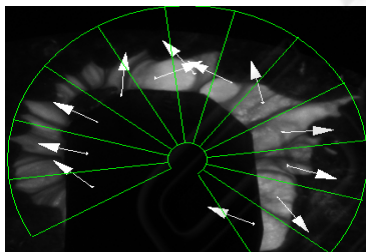

Figure 5: Sectors of active slag areas and detected flow.

For the final quantification of the slag motion, we have to determine if most of the slag is moving towards the electrode or in the opposite direction. For this purpose each vector direction is compared to the direction of the sector they belong to. The direction of a sector is simply the direction of the line bisecting the sector towards the centre of the electrode. If the absolute angular difference between a vector direction and the direction of its sector lays within a range of 0-60° the slag motion for this vector is "good", if the absolute difference is between 60° and 120° the slag motion is "undetermined" and otherwise the slag motion is "bad". For quantifying the overall slag motion in a given sector a majority voting is performed among the slag motion vectors belonging to the same sector.

4 CONCLUSIONS

We presented an experimental industrial vision system capable of measuring the slag temperature in a contactless manner with an accuracy of ± 5° C. By tracking the flow patterns of the slag, that system can also monitor and help assessing the quality of the produced steel. As future development we plan on investigating the relationship between the slag motion flow and its temperature in order to give the operator a better insight about the produced steel.

REFERENCES

Bouguet, J.-Y. (2000) 'Pyramidal Implementation of the Lucas Kanade Feature Tracker: Description of the Algorithm', *OpenCV Documents*, Intel Corporation, Microprocessor Research Labs.

Campbell, N. R.; Gardiner, H. W. B. (1925) 'Photo-electric colour-matching', *Journal of Scientific Instruments*, Vol. 2, Issue 6, pp. 177-187.

Lucas, B.D.; Kanade, T. (1981) 'An Iterative Image Registration Technique with an Application to Stereo Vision', *Proceedings of the 7th International Joint Conference on Artificial Intelligence*, pp. 674-679.

Meriaudeau, F.; Legrand, A.C.; Gorria, P. (2003) 'Real-time multispectral high-temperature measurement: application to control in the industry', *Proceedings of the SPIE*, Vol. 5011, pp. 234-242.

Otsu, N. (1979); 'A threshold selection method from gray-level histograms', *IEEE Transactions on Systems, Man and Cybernetics*, Vol. 9, pp. 62-66.

Urban, H.; Sidla, O. (2005); 'Online Temperature Measurement and Flow Analysis of Hot Dross in a Steel Plant', *Proceedings of the SPIE*, Vol. 6000, pp. 66-74.

Shi, J.; Tomasi C. (1994); 'Good Features to Track', *Proceedings of the IEEE Conference on Computer Vision and Pattern Recognition*, Vol. 1, pp593-600.

Simoncelli, E.P. (1994); 'Design of multi-dimensional derivative filters', *Proceedings of the IEEE Int. Conference on Image Processing*, Vol. 1, pp790-793.